Supporting Information

# Ultrastable Electrolyte (>3500 hours at High Current Density) Achieved by High-Entropy Solvation Toward Practical Aqueous Zinc Metal Batteries

Bin Xie[a#], Chaohe Zheng[b#], Haoran Lang[a], Min Li[a], Qiang Hu[*c], Xin Tan[*b], Qiaoji Zheng[a], Yu Huo[a], Jingxin Zhao[*d,e], Jia-Lin Yang[f], Zhen-Yi Gu[f], Dunmin Lin[*a], Xing-Long Wu*[f]

B. Xie, H. Lang, M. Li, Prof. Q. Zheng, Prof. Y. Huo, and Prof. D. Lin
College of Chemistry and Materials Science, Sichuan Normal University, Chengdu 610066, China
E-mail: ddmd222@sicnu.edu.cn

C. Zheng, and Prof. X. Tan
Institute for Carbon Neutralization Technology, College of Chemistry and Materials Engineering, Wenzhou University, Wenzhou 325035, Zhejiang, China
E-mail: xintan@wzu.edu.cn

Q. Hu
School of Materials and Energy University of Electronic Science and Technology of China, Chengdu 610054, China
E-mail: huqiang@std.uestc.edu.cn

Dr. J. Zhao
Nanotechnology Center, Research Institute for Intelligent Wearable Systems, The Hong Kong Polytechnic University, Hung Hom, Kowloon, Hong Kong 999077, P. R. China
E-mail: zjingxin@eduhk.hk

Dr. J. Zhao
School of Materials Science and Engineering, Xiangtan University, Xiangtan, 411105, P. R. China
E-mail: zjingxin@eduhk.hk

J.-L. Yang, Dr. Z.-Y. Gu and Prof. X.-L. Wu
MOE Key Laboratory for UV Light-Emitting Materials and Technology, Northeast Normal University, Changchun 130024, P.R. China
E-mail: xinglong@nenu.edu.cn

#B. Xie and C. Zheng contribute equally to this work.

## Experimental Section

### *Materials*

All chemicals were used directly without further purification. zinc sulfate ($ZnSO_4 \cdot 7H_2O$, ≥99.5 %, AR) were purchased from Chengdu Kolon Chemical Company， N, N-dimethylacetamide (DMAC, 99 %, AR) and $NH_4Ac$ (99%, GR) were purchased from Shanghai Maclean Biochemical Technology Company. Urea (≥99.5 %, AR) were purchased from Shanghai Aladdin Bio-Chem Technology.

### *Materials preparation*

*Preparation of cathode and anode*

The anode was made of purchased zinc foil (thickness 100 μm, 99.99%) with an abrasive material to remove the passivation layer. The zinc foil was then cut into discs (φ = 14 mm) to serve as zinc electrodes. The $NH_4V_4O_{10}$ was synthesized by a simple one-step hydrothermal reaction. In a typical synthesis, 0.354 g $NH_4V_3O_8$ was added to60 ml of distilled water and stirred for 1 h until completely dissolved. Then, 0.2835g of $H_2C_2O_4 \cdot 2H_2O$ was added to the solution, and stirred until completely dissolved. After that, the whole solution was transferred to a 100 mL PTFE-lined stainless-steel autoclave for a 24 h reaction at 180 °C. The powders were collected by centrifugation and washed 3 times with distilled water and absolute ethanol, and dried overnight in a vacuum oven at 60 °C. The $NH_4V_4O_{10}$ cathodes were prepared by mixing the active material, Super P carbon and polyvinylidene fluoride in a 7:2:1 weight ratio using N-methyl-2-pyrrolidone as a solvent. The slurry mixture was coated onto the Ti foil and dried under vacuum at 70℃ for 12 hours. The prepared electrodes were cut into circular pieces (φ = 10 mm) for use in coin-type cells.

*Preparation of HESE*

To prepare the $ZnSO_4$ electrolyte, 0.2 mol $ZnSO4 \cdot 7H_2O$ and deionized water were mixed in a 100 mL volumetric flask. High entropy electrolyte (HESE-1) was prepared by adding 0.01 mol urea, 5 vol % DMAC and 0.03 mol $NH_4Ac$ to 10 mL 2 M $ZnSO_4$ electrolyte. After experimental determination, the concentration of the mixed HESE was optimized, and the most concentrated electrolyte was HESE-0.5 electrolyte.

### *Materials characterization*

X-ray diffraction analysis (XRD) was characterized by equipment (Smart Lab, Riga ku, Japan) with a Cu-Kα (λ = 1.540598 Å, Smart Lab) source (scan rate of $4°min^{-1}$), with detected angular range of $2° < 2\theta < 80°$. The morphology of the samples was studied by field emission scanning electron microscopy (SEM, FEI, Sirion 200). The samples were characterized for elemental analysis using field emission scanning electron microscopy (SEM, FEI-Quanta 250, USA) and the corresponding energy dispersive x-ray (EDX) elemental mapping. The Bruker AVANCE AVIII 400 spectrometer was used to acquire the nuclear magnetic resonance (NMR) spectra of the electrolytes. The Fourier

transform infrared (FTIR) and Raman spectroscopy was used to acquire DGME exchange the solvation structure and adsorption behavior.

***Electrochemical evaluation***

The Zn||Zn symmetric cell, the Zn//Cu asymmetric cell and the Zn//NVO full cell were assembled in air to form a coin cell (CR2032). The batteries were assembled using a Zn plate (thickness of 100 μm) as the anode, electrolyte (200 μL), and glass fiber filters as the separator. The cycling performance of batteries was obtained by the LAND battery test system. The electrochemical impedance spectroscopy (EIS), cyclic voltammetry (CV), linear scanning voltammetry (LSV), Tafel profiles and chronoamperometry (CA) was performed on electrochemical workstations (CHI660E and CHI760E). The equivalent circuit of EIS fitting is R(C(RW)), and the equivalent circuit diagram is as follows:

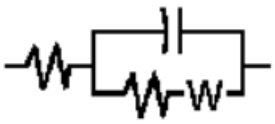


***Density functional theory (DFT) calculations***

The calculations for binding energy and deprotonation energy were conducted in Gaussian09 and ORCA software package.[1] The level B3LYP(D3)/6-31+g(d,p) was used for the optimized geometry, the energy calculations of combination of $Zn^{2+}$ and other molecules were performed under the ωB97M-V/def2TZVP level of theory while M06-2X(D3)/def2TZVP was used for evaluating weak interactions between organic molecules and water. In addition, the Solute Electron Density (SMD) implicit solvation model was used to describe the solvation effect.[2] The binding energies ($E_{binding}$) between two sections were calculated by

$$E_{binding} = E_{AB} - E_A - E_B$$

where $E_{AB}$ is the total energy of the complex, $E_A$ and $E_B$ are the energies of each fragment. For deprotonation reaction computation, we conducted further precise analysis on the $Zn^{2+}$ solvation clusters according to MD simulation results. The deprotonation energy for $H_2O$ in solvation clusters was computed by the following equation:

$$E_{deprotonation} = E_{cluster} - E_{H+} - E_{deprotonated\ cluster}$$

where $E_{H^+}$ is the absolute aqueous solvation free energy of the proton, $E_{cluster}$ and $E_{(deprotonated\ cluster)}$ are the energies of the cluster in the presence and absence of $H^+$ respectively.[3]

The calculations for entropy in electrolyte systems were implemented in CP2K and Shermo.[4, 5] Five system models were constructed preliminarily using the results of molecular dynamics simulation. System 1(2M $ZnSO_4$):5 $ZnSO_4$, 130 $H_2O$; System 2(2M $ZnSO_4$-Urea):5 $ZnSO_4$, 130 $H_2O$, 3 Urea; System 3(2M $ZnSO_4$-DMAC):5 $ZnSO_4$, 130 $H_2O$, 3 DMAC; System 4(2M $ZnSO_4$-$NH_4^+$/$AcO^-$):5 $ZnSO_4$, 130 $H_2O$, 2 $NH_4^+$,2 $AcO^-$; System 5(2M $ZnSO_4$-Urea/DMAC/$NH_4$+/$AcO^-$):5 $ZnSO_4$, 130 $H_2O$, 3

Urea, 3 DMAC, 2 $NH_4^+$, 2 $AcO^-$; The orbital transformation method was used for the wavefunction optimization and the plane wave cutoff was set to 600 Ry. The basis set was DZVP-MOLOPT-SR-GTH level and the core electrons were represented by Goedecker-Teter-Hutter (GTH) pseudopotentials.[6] Perdew-Burke-Ernzerhof (PBE) functional was used to describe the exchange-correlation effects. The geometries were optimized by Broyden-Fletcher-Goldfarb-Shanno (BFGS) minimizer and the structural optimization parameter of max force was set to $1\times10^{-5}$.[7, 8] The entropy of the electrolyte was ultimately determined by analyzing the frequency results of the optimized structure.

***Molecular Dynamics (MD) simulations***

The classical MD simulations were performed in the Large Scale Atomic/Molecular Massively Parallel Simulator (LAMMPS). [9] The MD parameters for all molecules were obtained from OPLS-AA force fields and set up by Moltemplate while SPC/E model was applied to water.[10] To avoid the impact of overestimating charges on the simulation, the charge of ions in the electrolyte was reduced proportionally in all cases according to the method proposed by Vega and Acevedo ($Zn^{2+}$ and $SO_4^{2-}$ scaled by 0.85, $NH_4^+$ and $AcO^-$ scaled by 0.8).[11, 12] The particle-particle particle-mesh solver (PPPM) was applied in long-range electrostatic interactions. A cut-off distance of 1.2 nm was used for electrostatic and 12-6 Lennard-Jones interactions.

For electrolyte structure determination, a canonical (NVT) ensemble for 1 ns was applied firstly to 2 M $ZnSO_4$ (60 $ZnSO_4$, 1200 $H_2O$) and 2 M $ZnSO_4$-Urea/DMAC/$NH_4^+$/$AcO^-$ (60 $ZnSO_4$, 1200 $H_2O$, 40 Urea, 40DMAC, 20 $NH_4^+$, 20$AcO^-$) electrolyte systems. The experimental system was then subjected to two cycles of quench-annealing dynamics which the temperature was cycled between 298 K and 500 K to drive the system to reach the lowest potential energy. After that two systems were equilibrated under an isothermal-isobaric (NPT) ensemble for 10 ns at a temperature of 298 K and a pressure of 1 atm with a time step of 1 fs. Finally, another 10 ns simulation was performed in the NVT ensemble under Nose-Hoover thermostats at 298 K to analyze the radial distribution function (RDF) of the system.

For surface energy calculation, simulation boxes contain molecular model of $ZnSO_4$ electrolyte with or without additives which is exposed to zinc metal surface at 30×30 $Å^2$. The MEAM potential was applied to zinc metal while Lennard-Jones potential was used to describe the interactions between zinc metal and liquid molecules.[13] The surface energy of zinc metal crystal faces (002) (100) (101) in solution environment ($E_{surf}$) was defined as:

$$E_{surf} = \gamma_s + \frac{E_{sol}}{2A}$$

Where $\gamma_s$ is the surface energy of metal crystal planes under vacuum conditions which was evaluated by dividing metals to form new crystal planes, $E_{sol}$ is the interaction energy between the solution and the crystal plane which was obtained by built-in commands during simulation while A is the area of contact between them. All the snapshots of the MD simulations were implemented by VMD software.[14]

***The activation energy is calculated from the Arrhenius equation***

$$\frac{1}{R_{ct}} = Aexp(-\frac{E_a}{RT})$$

Where Rct is the charge transfer resistance (Ω), A is the pre-exponential factor, Ea is the activation energy (KJ $mol^{-1}$), R is the gas constant (8.314J $(mol*K)^{-1}$), T is the Kelvin temperature (K).

***The (cumulative plating capacity) CPC calculation formula***

Cumulative plating capacity = area capacity × cycle number

In this work, the symmetric cells are used to cycle more than 1750 cycles at 5 mA $cm^{-2}$ and 5 mAh $cm^{-2}$, thus the CPC is 5 mAh $m^{-2}$ ×1750 cycles, and the result is 8750 mAh $cm^{-2}$.

## Supporting Figures

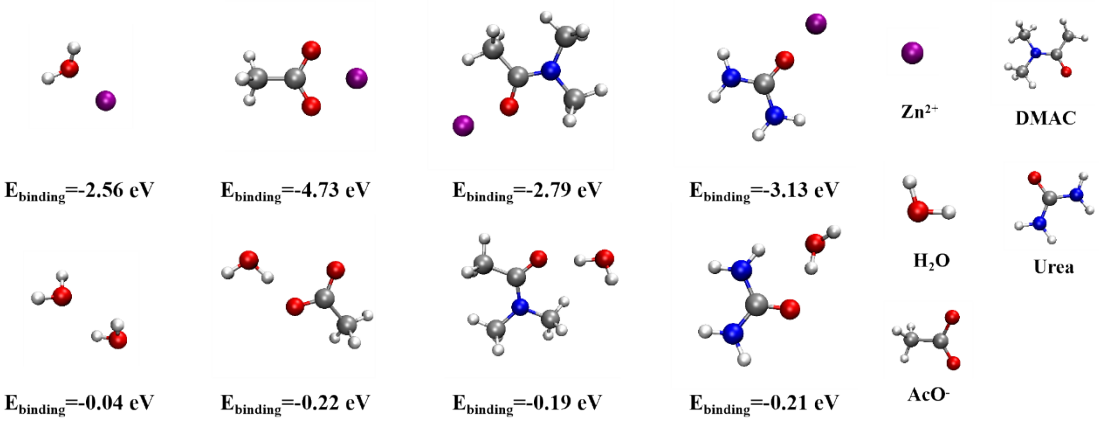


**Figure S1.** The binding energies between different additive molecules and $Zn^{2+}$ or water.

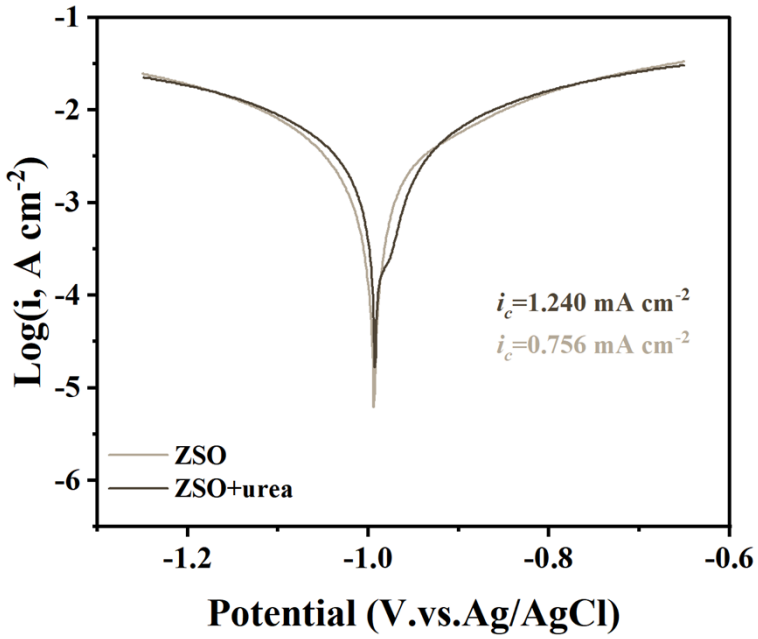


**Figure S2.** The Tafel curves and corresponding corrosion current density in ZSO and urea electrolytes.

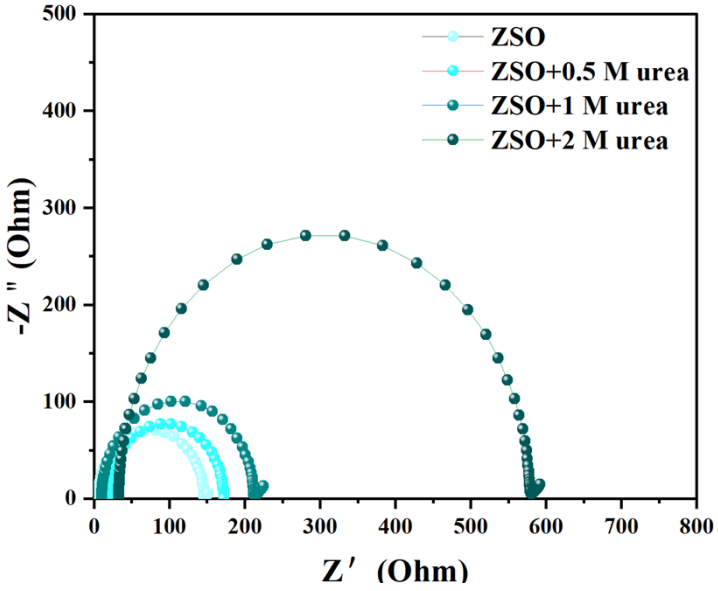


**Figure S3.** Nyquist EIS plots at different concentrations in ZSO+urea.

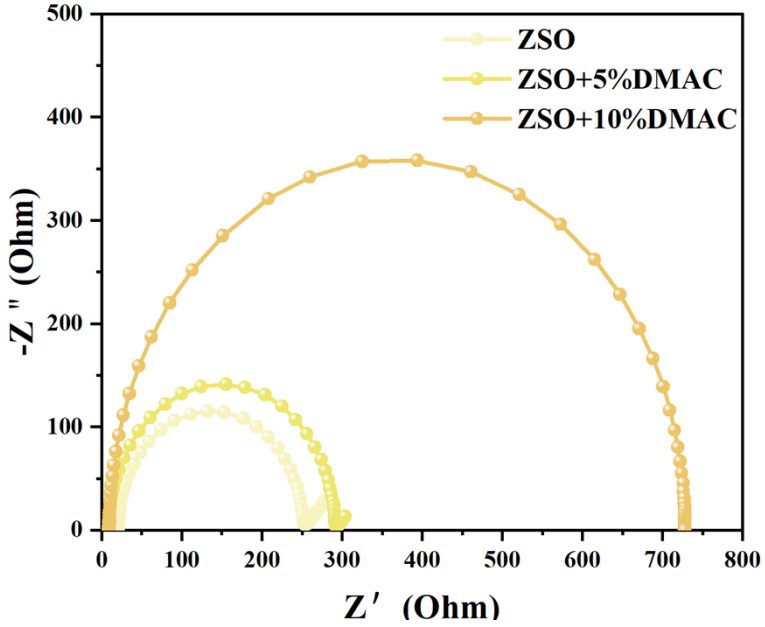


**Figure S4.** Nyquist EIS plots at different concentrations in ZSO+DMAC.

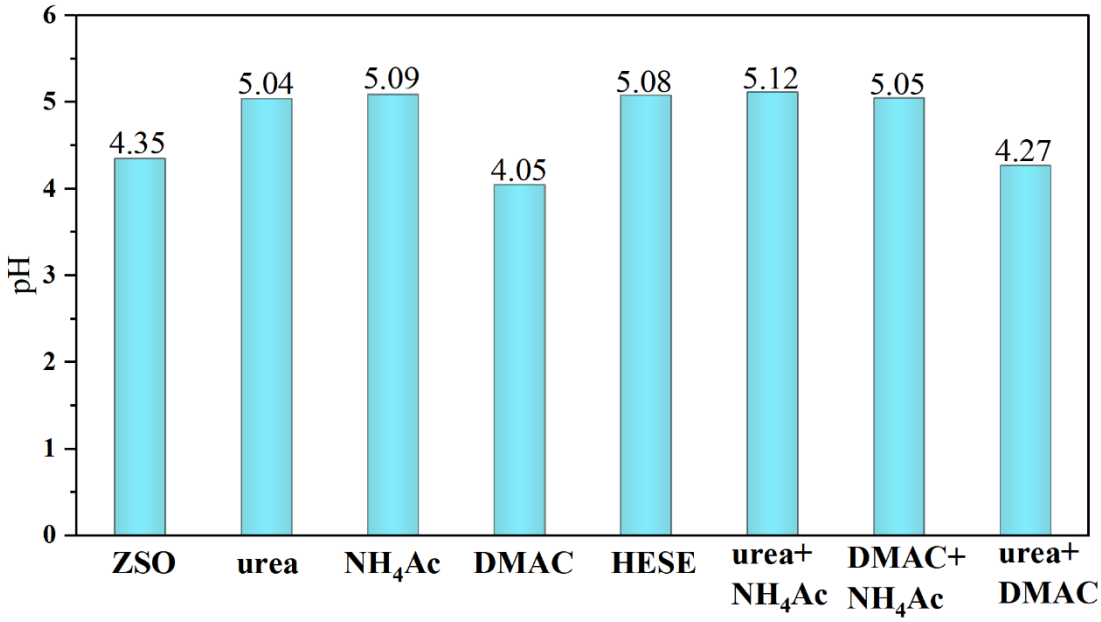


**Figure S5.** pH value of different electrolytes.

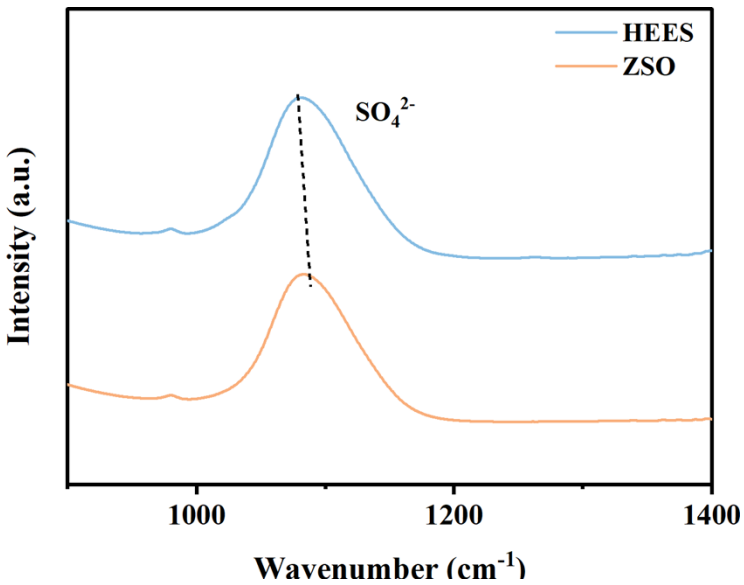


**Figure S6.** The v-$SO_4^{2-}$ stretching in different electrolytes.

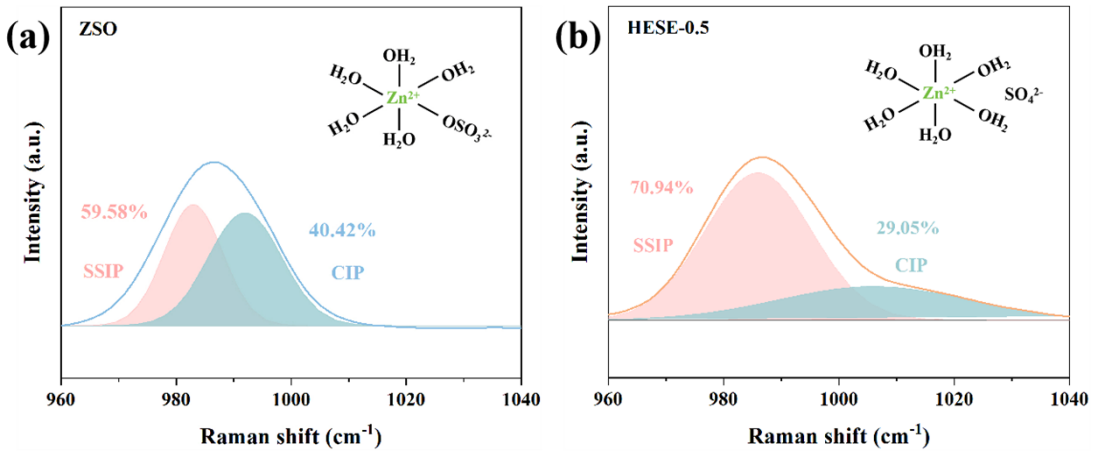


**Figure S7.** Fitted Raman spectra of $SO_4^{2-}$ vibration band in (a) ZSO and (b) HESE electrolytes.

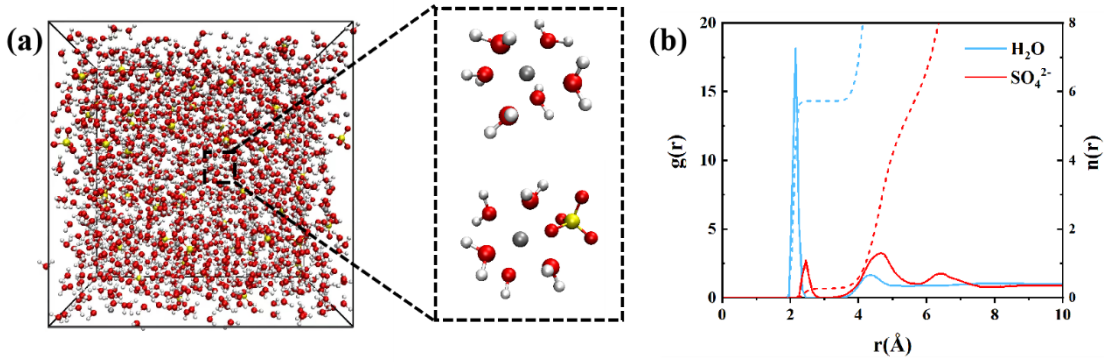


**Figure S8.** (a) The MD simulation snapshot and the representative solvation structure of $Zn^{2+}$ in ZSO electrolyte. (b) RDFs and the corresponding coordination numbers.

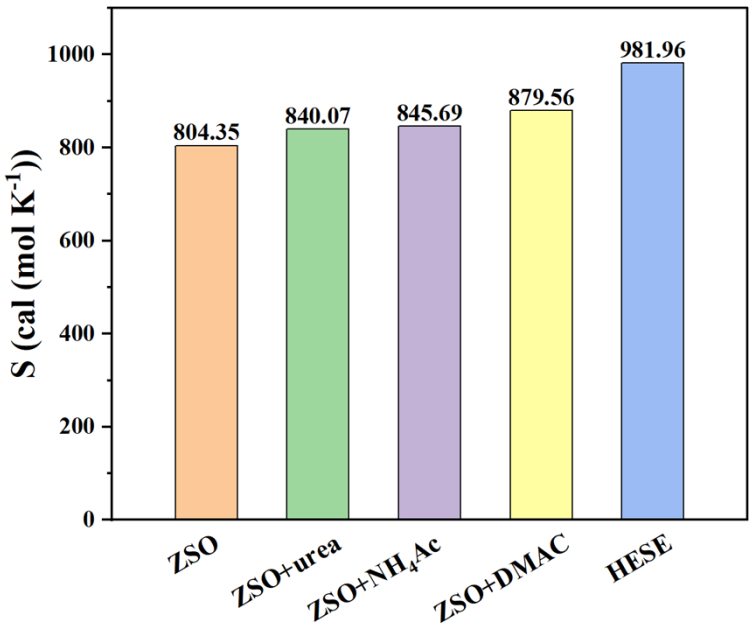


**Figure S9** The calculated entropy in different electrolytes.

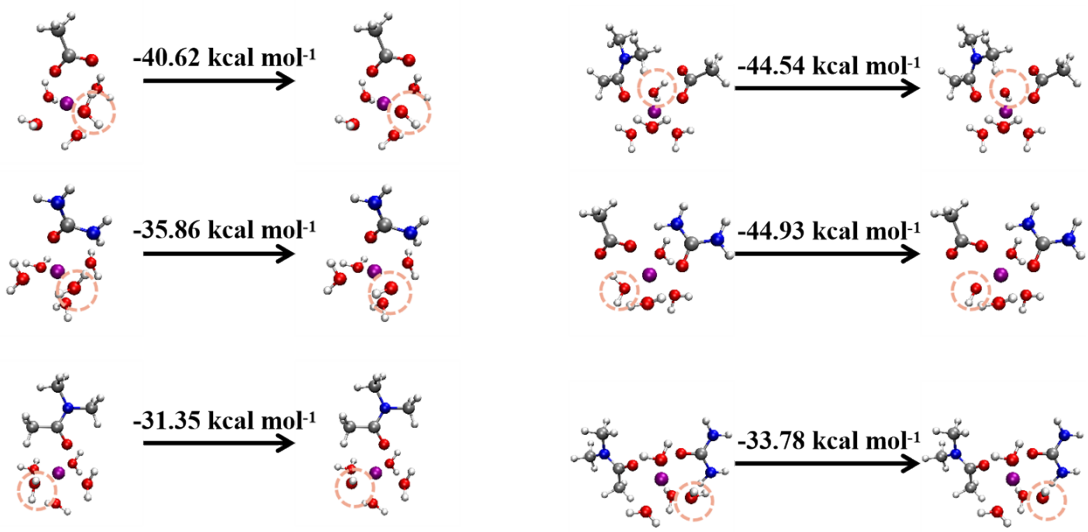


**Figure S10.** Deprotonation energies of different solvation structures.

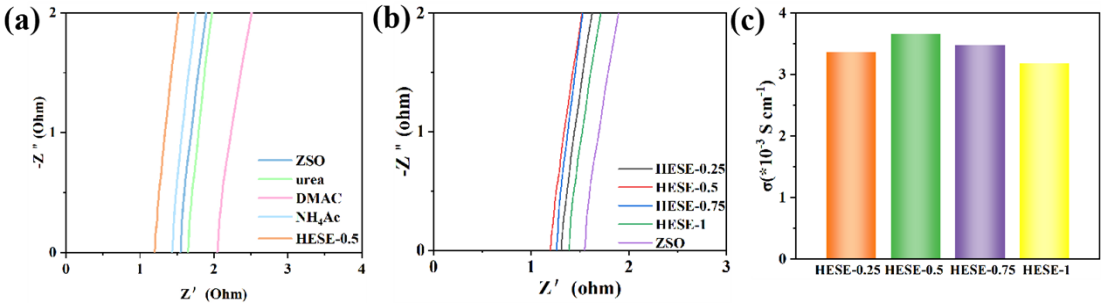


**Figure S11.** The Nyquist plots of the symmetric cells with (a) different electrolytes, (b) with different concentration of HESE and (c) corresponding ionic conductivity.

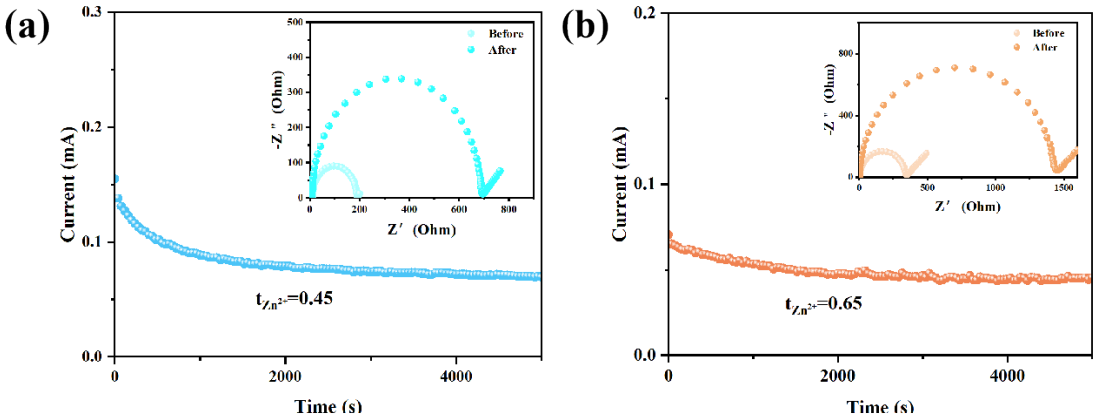


**Figure S12.** I-t curves in (a) ZSO and (b) HESE electrolytes at a potential step of 25 mV. The electrochemical impedance spectra of Zn||Zn symmetrical cells before and after polarization test in ZSO and HESE electrolytes were included.

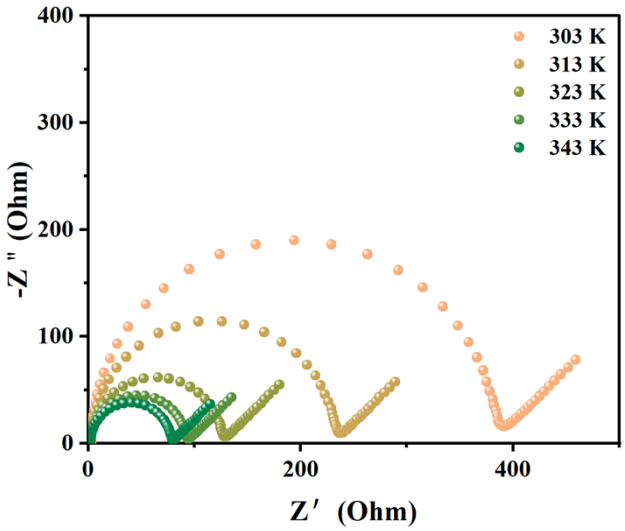


**Figure S13.** The Nyquist plots of Zn||Zn symmetric cells with ZSO electrolyte at different temperatures.

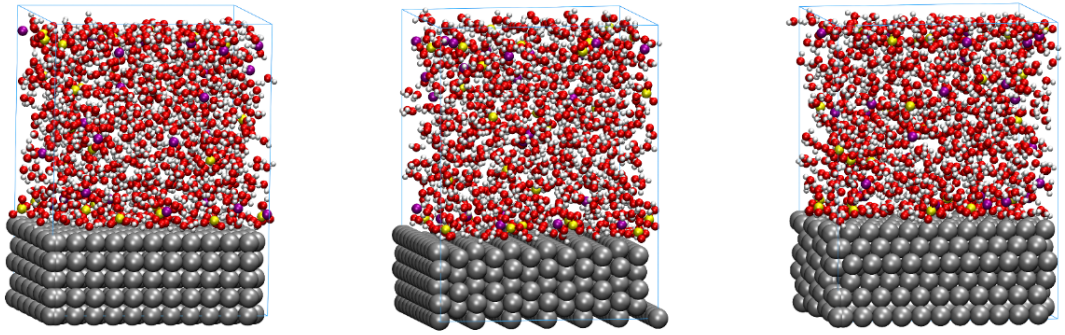

**(002) plane**
**$E_{surf}$=0.098 J m$^{-2}$**

**(100) plane**
**$E_{surf}$=0.149 J m$^{-2}$**

**(101) plane**
**$E_{surf}$=0.114 J m$^{-2}$**

**Figure S14.** The simulation models and surface energies of (002), (100) and (101) crystal planes in ZSO electrolyte.

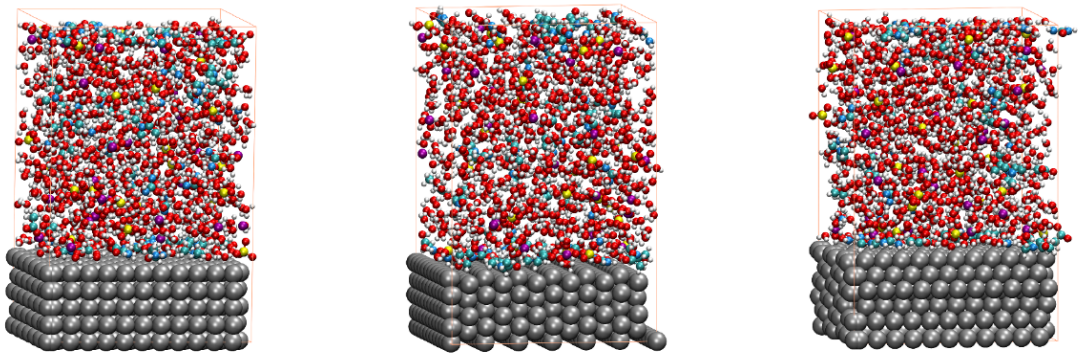


**Figure S15.** The simulation models and surface energies of (002), (100) and (101) crystal planes in HESE.

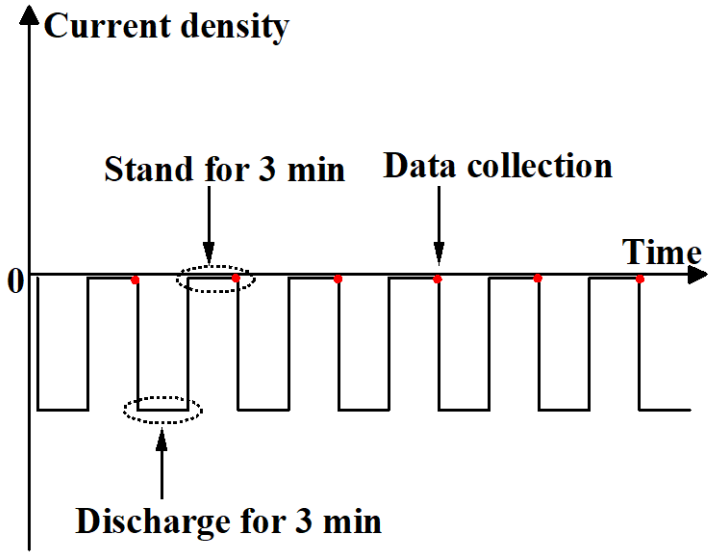


**Figure S16.** Schematic illustration of in situ electrochemical impedance spectroscopy process.

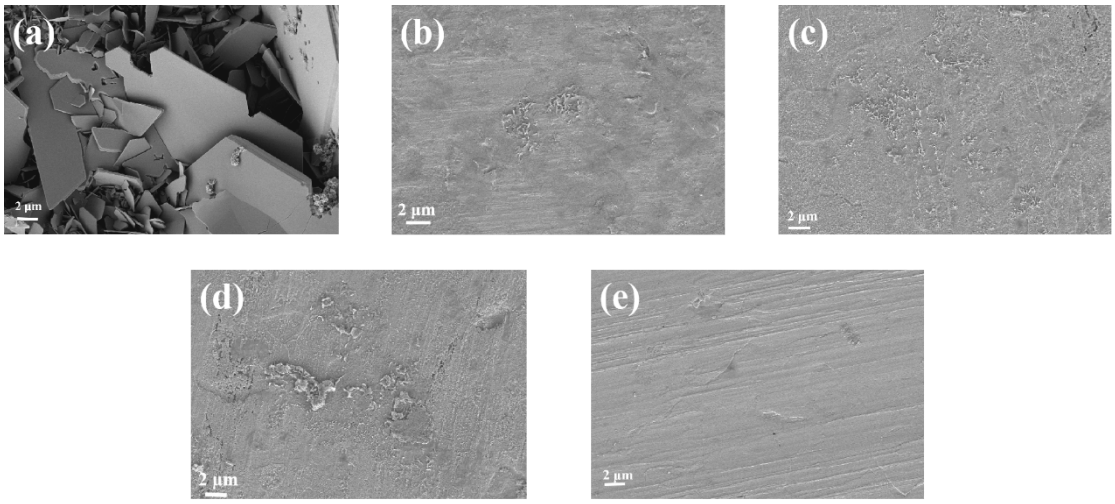


**Figure S17.** SEM images of soaking in ZSO electrolyte with (a) urea, (b) $NH_4Ac$ and (c) DMAC for 10 days.

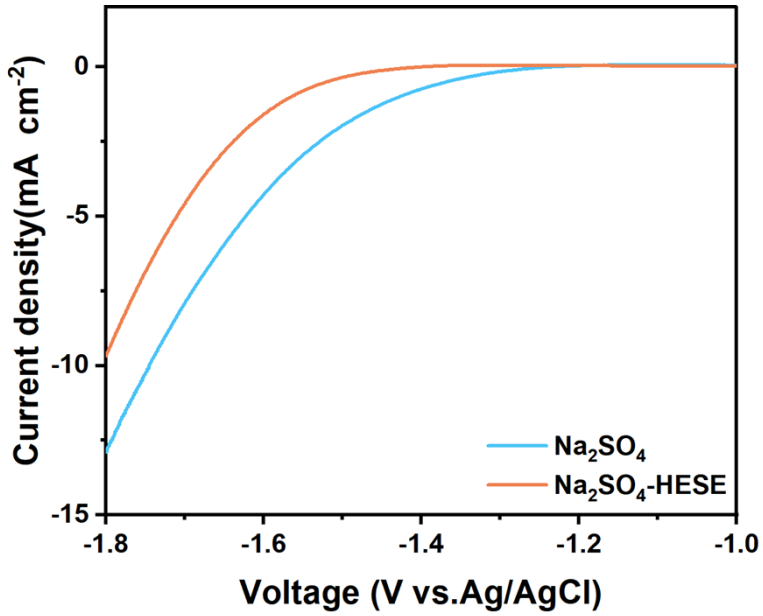


**Figure S18.** Linear sweep voltammetry curves of zinc anodes tested using a three-electrode system in 2M $Na_2SO_4$ electrolytes with/without additive

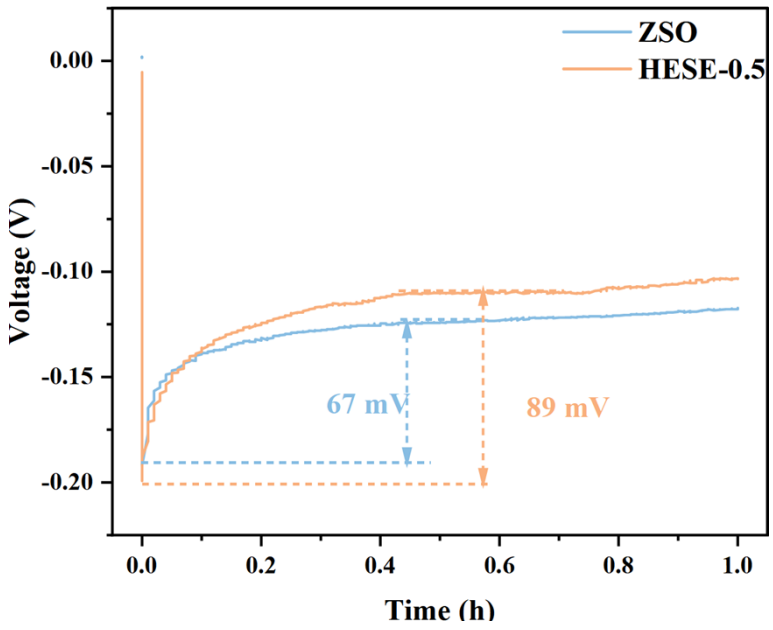


**Figure S19.** Zinc deposition overpotential in ZSO and HESE electrolytes at a current density of 5 mA $cm^{-2}$.

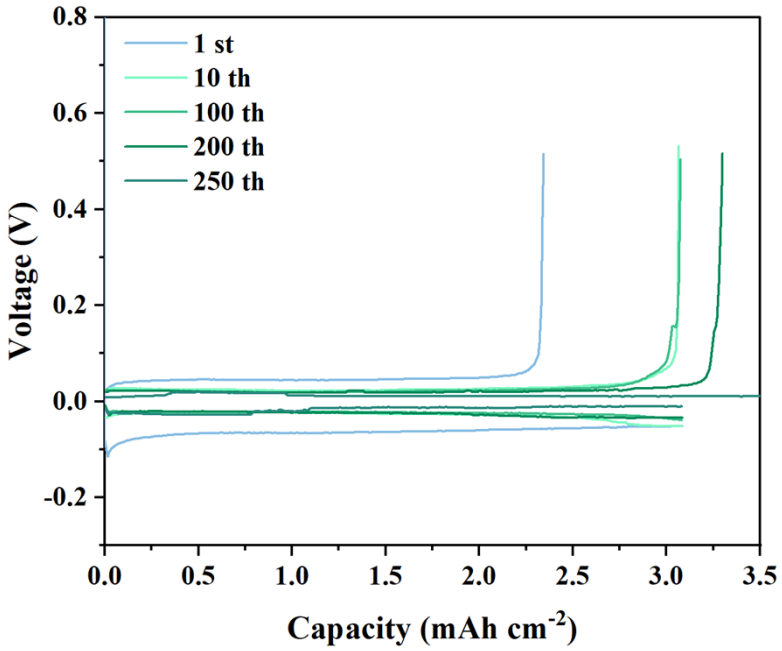


**Figure S20.** Voltage profiles of Zn//Cu asymmetric cells in ZSO electrolyte.

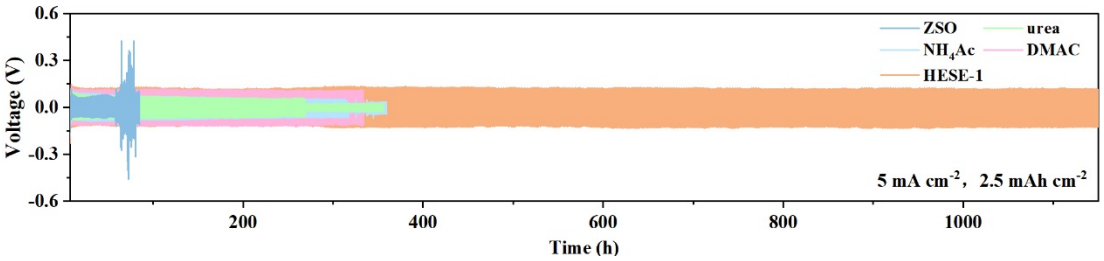


**Figure S21.** Long cycle performance of Zn||Zn symmetric cells with different additives at 5 mA $cm^{-2}$/2.5mAh $cm^{-2}$.


**Figure S22.** Optical photos of different concentrations of HESE electrolyte.

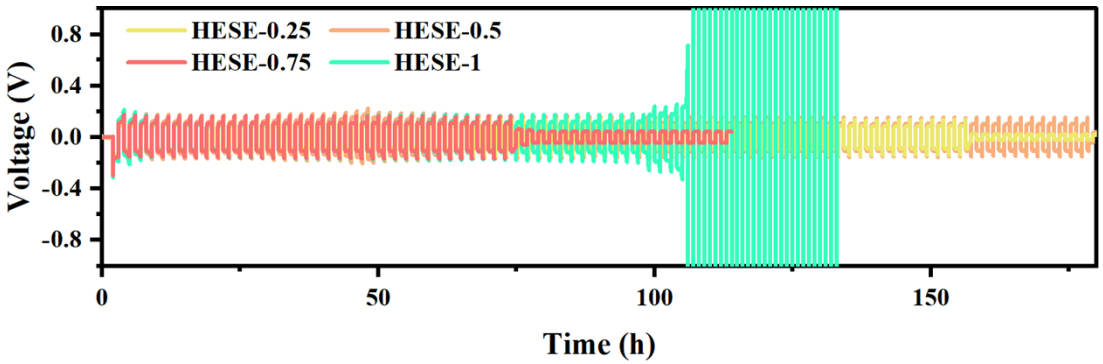


**Figure S23.** The cycling performance of Zn||Zn symmetric cells with different concentrations of HESE electrolyte at 20 mA $cm^{-2}$ and 20 mAh $cm^{-2}$.

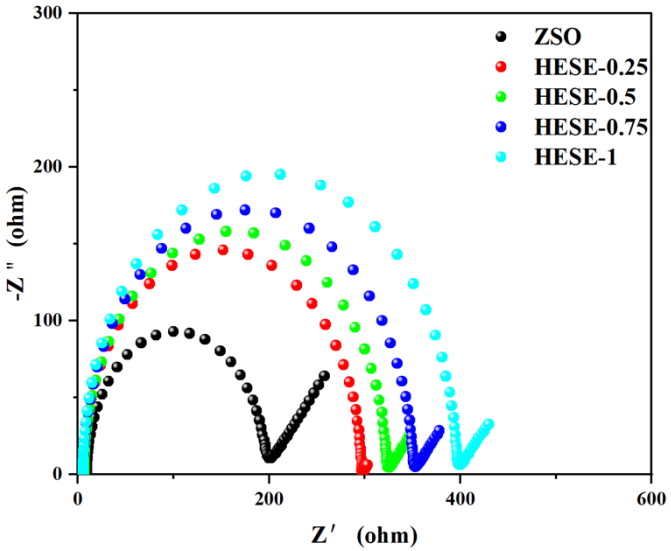


**Figure S24.** EIS curves of Zn//Zn symmetric cells at different concentrations

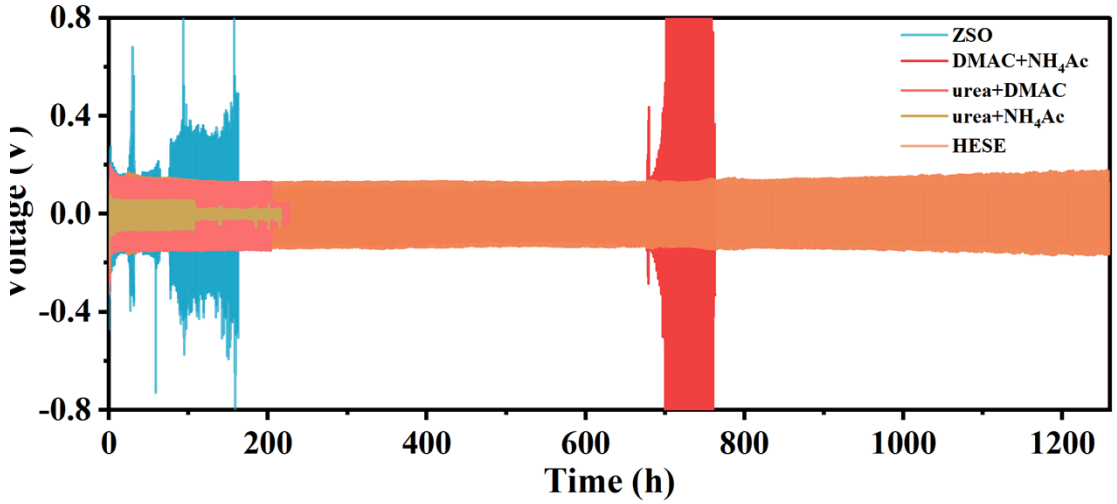


**Figure S25.** The long cycle performance of Zn||Zn symmetric batteries with different concentrations of HESE electrolyte at 10 mA $cm^{-2}$ and 10 mAh $cm^{-2}$.

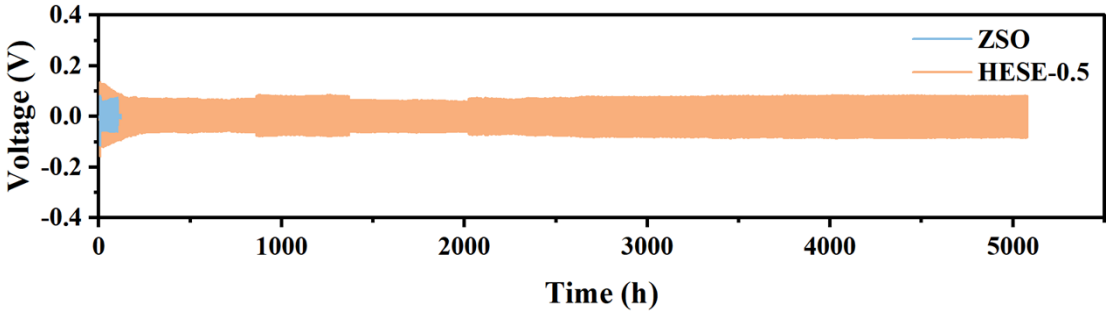


**Figure S26.** The long cycle performance of Zn||Zn symmetric batteries with different concentrations of HESE electrolyte at 0.5 mA $cm^{-2}$ and 0.25 mAh $cm^{-2}$.

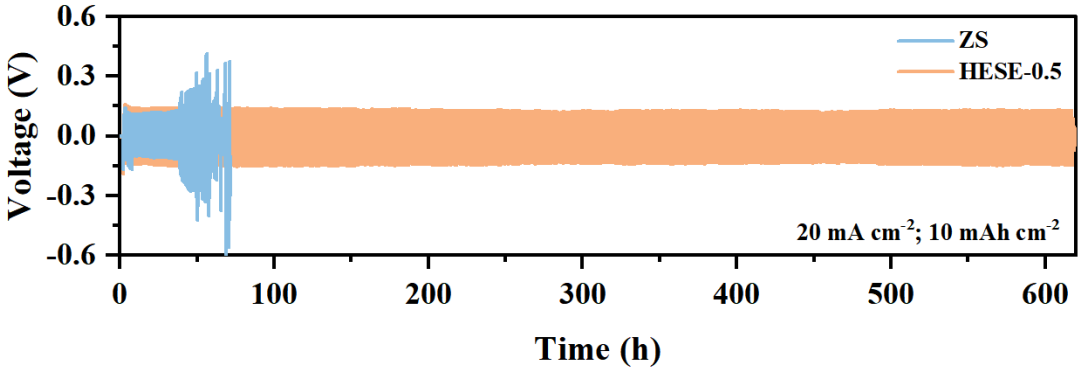


**Figure S27.** The long cycle performance of Zn||Zn symmetric batteries with different concentrations of HESE electrolyte at 20 mA $cm^{-2}$ and 10 mAh $cm^{-2}$.

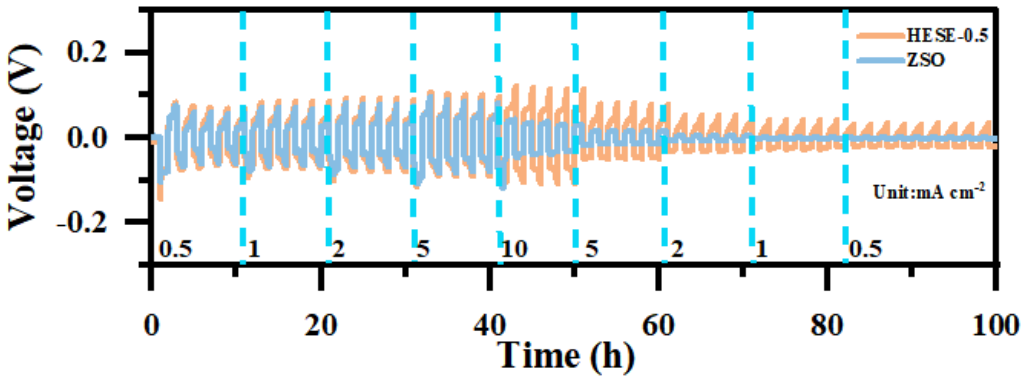


**Figure S28.** Rate performance of Zn||Zn symmetric cells at different current densities ranging from 0.5 to 10 mA $cm^{-2}$ in two electrolytes.

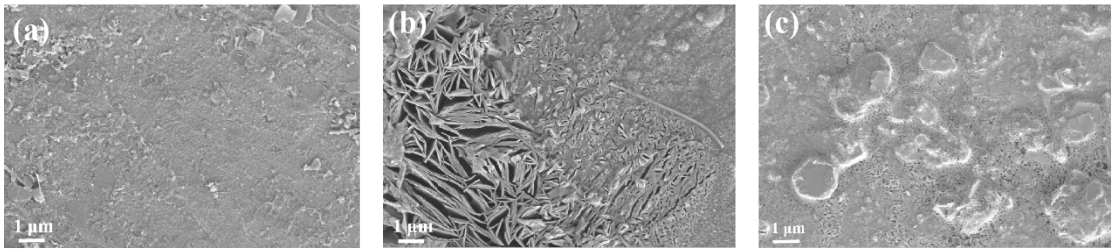


**Figure S29.** The anode SEM after 50 cycles in a symmetrical battery containing ZSO electrolyte with (a) DMAC, (b) $NH_4Ac$ and (c) urea.

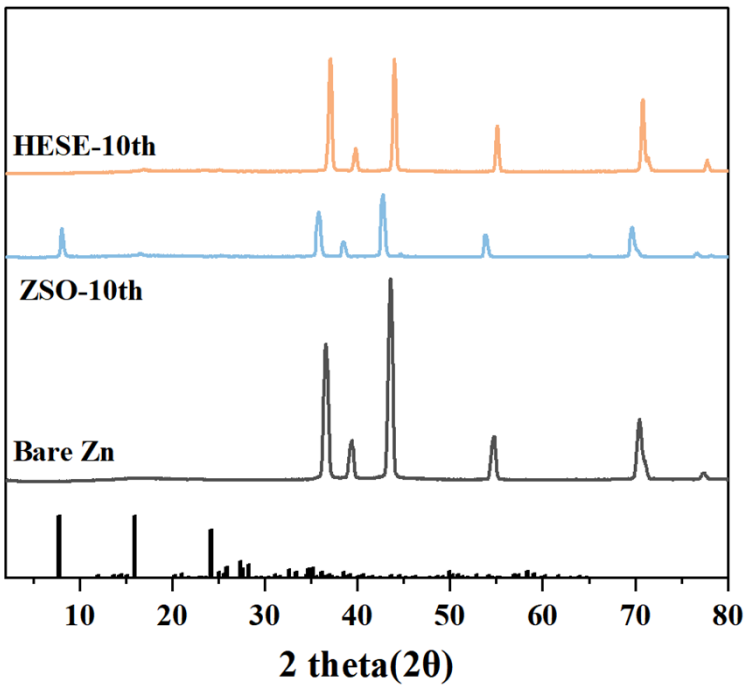


**Figure S30.** The anode XRD pattern after 50 cycles in a symmetrical battery containing ZSO and HESE electrolytes.

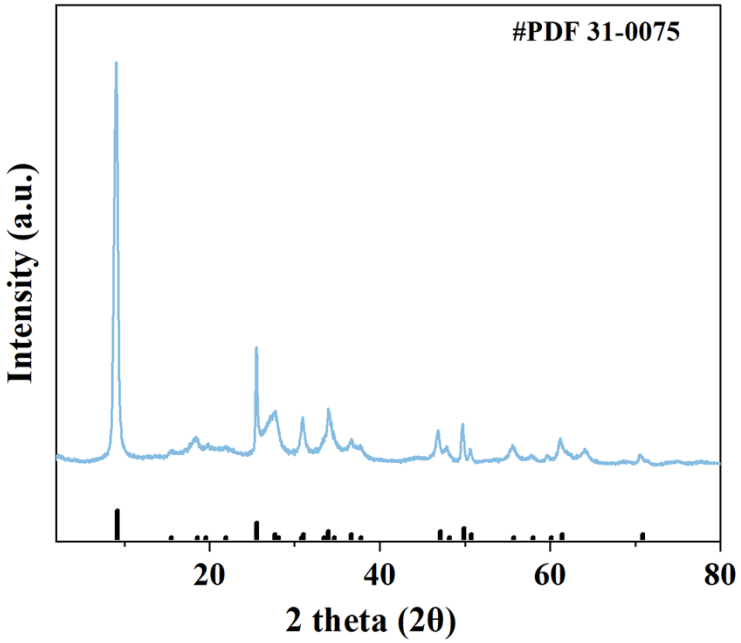


**Figure S31.** XRD pattern of NVO anode material.

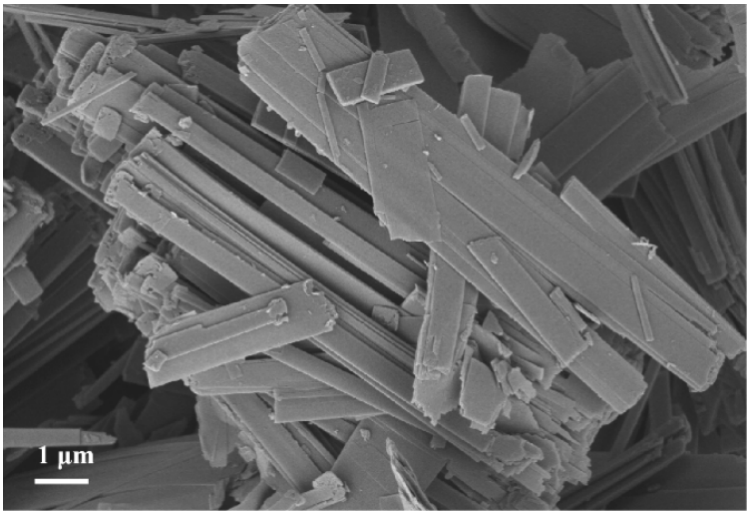


**Figure S32.** SEM of NVO cathode material.

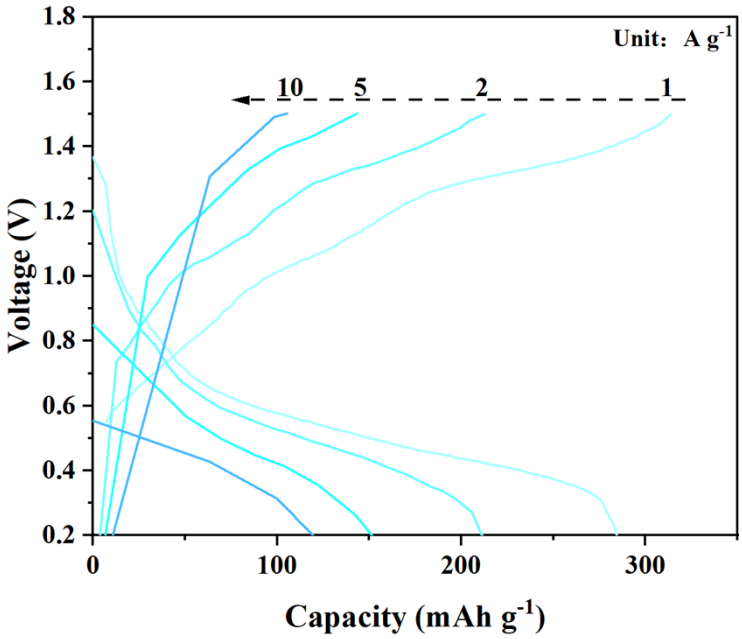


**Figure S33.** The GCD curves of Zn//NVO cells in ZSO electrolyte.

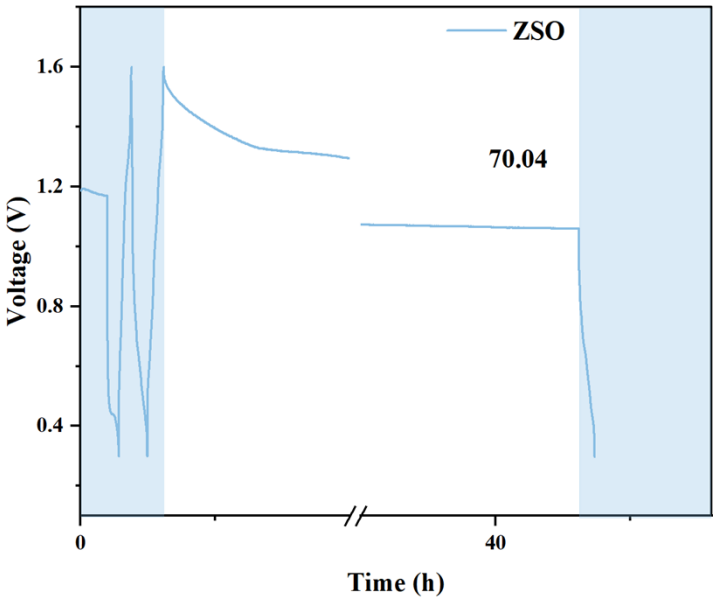


**Figure S34.** The self-discharge behavior of batteries in ZSO electrolytes.

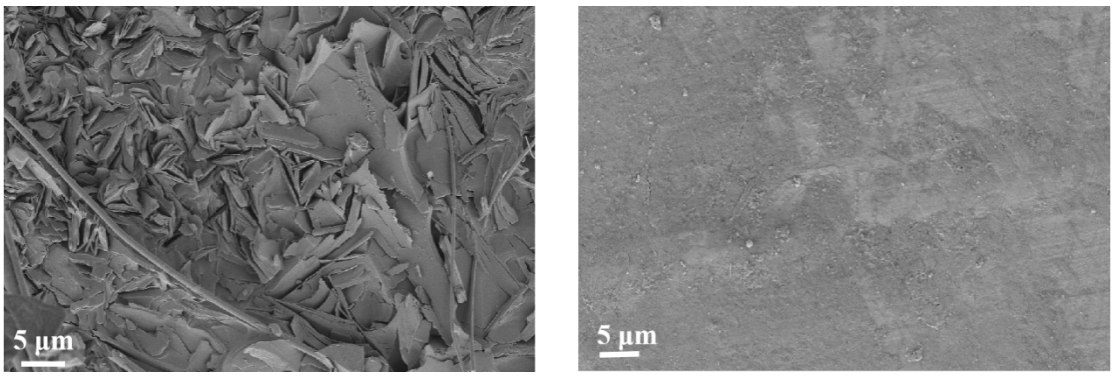


**Figure S35.** SEM images of Zn anode of Zn//NVO battery a) cycled for 50 times in ZSO electrolyte, b) cycled for 50 times in HESE.

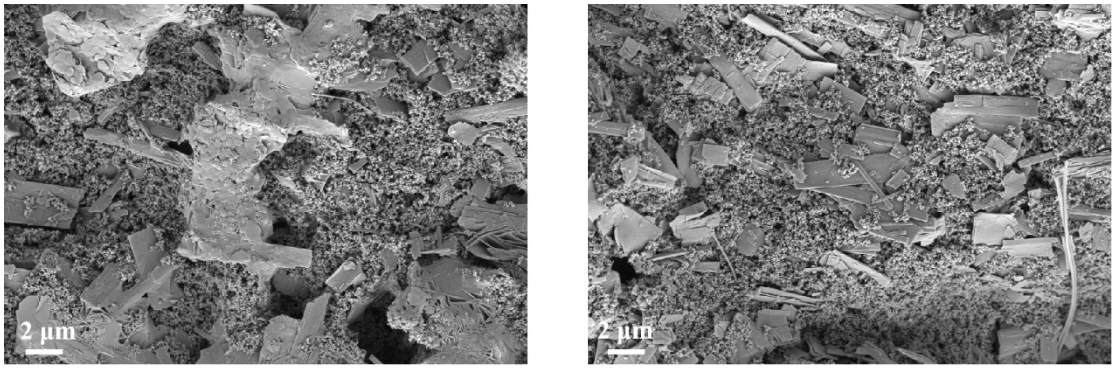


**Figure S36.** SEM images of NVO cathode of Zn//NVO battery a) cycled 50 times in ZSO electrolyte, b) cycled 50 times in HESE.

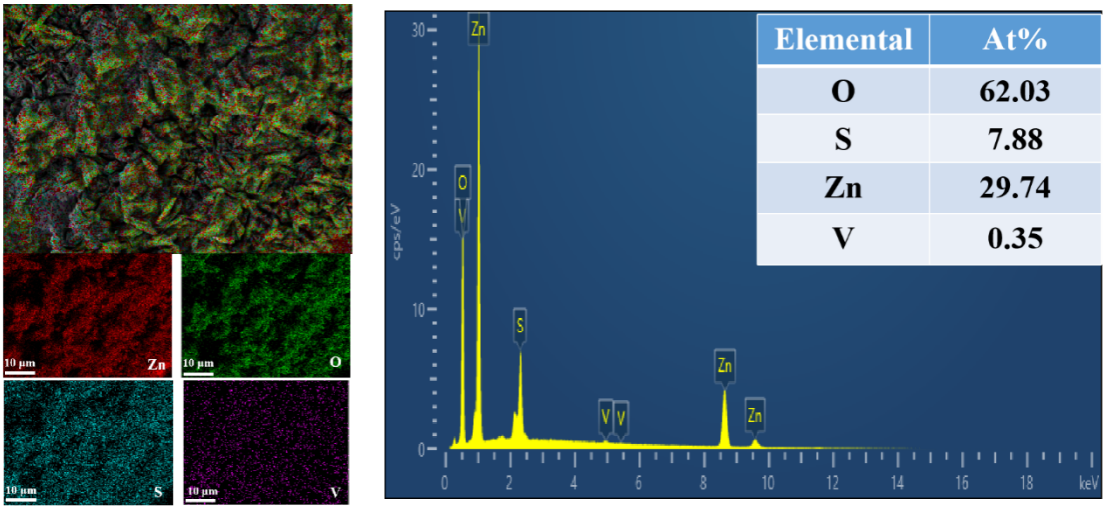


**Figure S37.** Map Sum Spectrum and EDS mapping of Zn anode in a Zn//NVO full cell using ZSO electrolyte after 50 cycles.

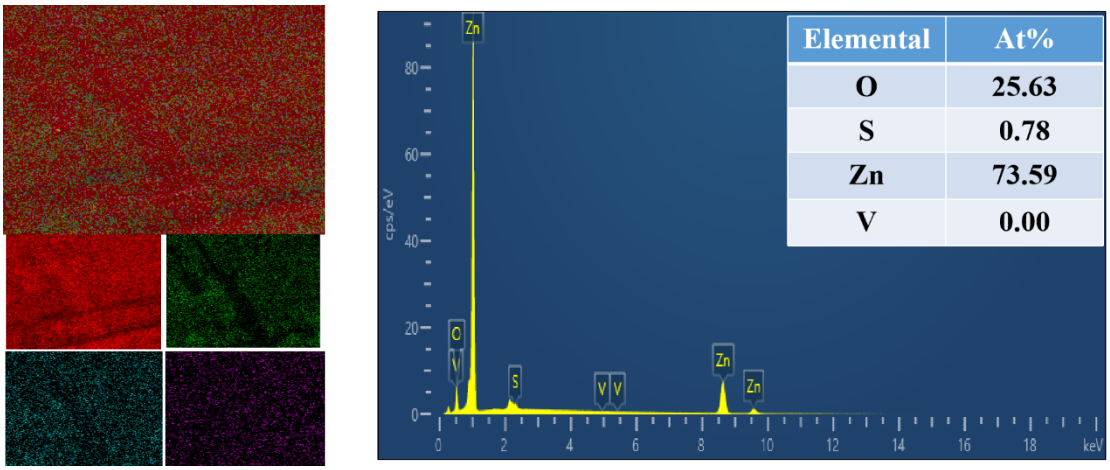


| Elemental | At% |
|---|---|
| O | 25.63 |
| S | 0.78 |
| Zn | 73.59 |
| V | 0.00 |

**Figure S38.** Map Sum Spectrum and EDS mapping of Zn anode in a Zn//NVO full cell using HESE after 50 cycles.

**Table S1：** The electrochemical performance of ZMBs in this study was compared with that of previously reported electrolytes.

| Electrolytes | Symmetric Zn cells | | | Asymmetric Zn cells | Ref. |
|---|---|---|---|---|---|
| | Current Density (mA/cm$^2$) /Capacity (mAh/cm$^2$ ) | Lifespan (h) | CPC (mAh/cm$^2$) | Average CE (%) | |
| HESE (this work) | 5/5<br>10/10 | 3500<br>1300 | 8750<br>6500 | 99.76 | — |
| $BMIm^+$ | 5/5<br>10/10 | 1400<br>1000 | 3500<br>5000 | 99.8 | [15] |
| ET | 1/1<br>5/5 | 5700<br>2000 | 2850<br>5000 | 99.6 | [16] |
| NMI | 1/1 | 2600 | 1300 | 99.74 | [17] |
| L-CN | 1/1 | 6083 | 3041.5 | 98..85 | [18] |
| $CH_3OH$ | 5/5 | 1000 | 2500 | 99.5 | [19][18] |
| DMAC+TMP | 5/5 | 1600 | 4000 | 99.5 | [20][19] |
| $SrTiO_3$ | 1/0.5<br>2/1 | 2000<br>2000 | 1000<br>2000 | 99 | [21] |
| N -ac | 10/10<br>2/2 | 1200<br>3100 | 6000<br>3100 | 99.81 | [22] |
| Tris | 3/1 | 2600 | 3940 | 99.2 | [23] |
| HMPA | 10/10 | 500 | 2500 | 99.4 | [24] |
| $Y^{3+}$ | 5/2 | 2100 | 6000 | 98.4 | [25] |
| Azi | 10/10<br>1/1 | 1000<br>4000 | 5000<br>2000 | 99.1 | [26] |

References

[1] F. Neese, *WIREs Computational Molecular Science* **2022**, *12*, e1606.

[2] A. V. Marenich, C. J. Cramer, D. G. Truhlar, *The Journal of Physical Chemistry B* **2009**, *113*, 6378.

[3] C. P. Kelly, C. J. Cramer, D. G. Truhlar, *The Journal of Physical Chemistry B* **2006**, *110*, 16066.

[4] T. D. Kuhne, M. Iannuzzi, B. M. Del, V. V. Rybkin, P. Seewald, F. Stein, T. Laino, R. Z. Khaliullin, O. Schutt, F. Schiffmann, D. Golze, J. Wilhelm, S. Chulkov, M. H. Bani-Hashemian, V. Weber, U. Borstnik, M. Taillefumier, A. S. Jakobovits, A. Lazzaro, H. Pabst, T. Muller, R. Schade, M. Guidon, S. Andermatt, N. Holmberg, G. K. Schenter, A. Hehn, A. Bussy, F. Belleflamme, G. Tabacchi, A. Gloss, M. Lass, I. Bethune, C. J. Mundy, C. Plessl, M. Watkins, J. VandeVondele, M. Krack, J. Hutter, *J. Chem. Phys.* **2020**, *152*, 194103.

[5] T. Lu, Q. Chen, *Comput. Theor. Chem.* **2021**, *1200*, 113249.

[6] S. Goedecker, M. Teter, J. Hutter, *Physical review. B, Condensed matter* **1996**, *54*, 1703.

[7] J. P. Perdew, K. Burke, M. Ernzerhof, *Phys. Rev. Lett.* **1996**, *77*, 3865.

[8] Y. Dai, *SIAM J. Optim.* **2002**, *13*, 693.

[9] A. P. Thompson, H. M. Aktulga, R. Berger, D. S. Bolintineanu, W. M. Brown, P. S. Crozier, P. J. In T Veld, A. Kohlmeyer, S. G. Moore, T. D. Nguyen, R. Shan, M. J. Stevens, J. Tranchida, C. Trott, S. J. Plimpton, *Comput. Phys. Commun.* **2022**, *271*, 108171.

[10] W. L. Jorgensen, D. S. Maxwell, J. Tirado-Rives, *J. Am. Chem. Soc.* **1996**, *118*,

11225.

[11] I. M. Zeron, J. L. F. Abascal, C. Vega, *The Journal of Chemical Physics* **2019**, *151*.

[12] B. Doherty, X. Zhong, S. Gathiaka, B. Li, O. Acevedo, *J. Chem. Theory Comput.* **2017**, *13*, 6131.

[13] H. Jang, K. Kim, B. Lee, *Calphad-Comput. Coupling Ph. Diagrams Thermochem.* **2018**, *60*, 200.

[14] W. Humphrey, A. Dalke, K. Schulten, *J Mol Graph* **1996**, *14*, 33, 27.

[15] H. Zhang, Y. Zhong, J. Li, Y. Liao, J. Zeng, Y. Shen, L. Yuan, Z. Li, Y. Huang, *Adv. Energy Mater.* **2023**, *13*, 2203254.

[16] Q. Meng, Q. Bai, R. Zhao, P. Cao, G. Zhang, J. Wang, F. Su, X. Zhou, J. Yang, J. Tang, *Adv. Energy Mater.* **2023**, *13*, 202302828.

[17] M. Zhang, H. Hua, P. Dai, Z. He, L. Han, P. Tang, J. Yang, P. Lin, Y. Zhang, D. Zhan, J. Chen, Y. Qiao, C. C. Li, J. Zhao, Y. Yang, *Adv. Mater.* **2023**, *35*, 2208630.

[18] H. Yu, D. Chen, X. Ni, P. Qing, C. Yan, W. Wei, J. Ma, X. Ji, Y. Chen, L. Chen, *Energy Environ. Sci.* **2023**, *16*, 2684.

[19] W. Xu, J. Li, X. Liao, L. Zhang, X. Zhang, C. Liu, K. Amine, K. Zhao, J. Lu, *J. Am. Chem. Soc.* **2023**, *145*, 22456.

[20] Y. Wang, Z. Wang, W. K. Pang, W. Lie, J. A. Yuwono, G. Liang, S. Liu, A. M. D. Angelo, J. Deng, Y. Fan, K. Davey, B. Li, Z. Guo, *Nat. Commun.* **2023**, *14*, 2720.

[21] R. Deng, Z. He, F. Chu, J. Lei, Y. Cheng, Y. Zhou, F. Wu, *Nat. Commun.* **2023**, *14*, 4981.

[22] D. Xu, X. Ren, H. Li, Y. Zhou, S. Chai, Y. Chen, H. Li, L. Bai, Z. Chang, A. Pan, H. Zhou, *Angew. Chem. Int. Ed.* **2024**, *63*, e202402833.

[23] M. Han, J. Zhang, C. Yu, J. Yu, Y. Wang, Z. Jiang, M. Yao, G. Xie, Z. Yu, J. Qu, *Angew. Chem. Int. Ed.* **2024**, *63*, e202403695.

[24] D. Wang, D. Lv, H. Peng, C. Wang, H. Liu, J. Yang, Y. Qian, *Angew. Chem. Int. Ed.* **2023**, *62*, e202310290.

[25] Y. Ding, X. Zhang, T. Wang, B. Lu, Z. Zeng, Y. Tang, J. Zhou, S. Liang, *Energy Storage Mater.* **2023**, *62*, 102949.

[26] X. Bai, Y. Nan, K. Yang, B. Deng, J. Shao, W. Hu, X. Pu, *Adv. Funct. Mater.* **2023**, *33*, 2307595.